Chaos, Symmetry, and Self-Similarity: Exploiting Order and Disorder in Mixing Processes

J. M. Ottino, F. J. Muzzio, M. Tjahjadi, J. G. Franjione, S. C. Jana, H. A. Kusch

Fluid mixing is a successful application of chaos. Theory anticipates the coexistence of order and disorder—symmetry and chaos—as well as self-similarity and multifractality arising from repeated stretching and folding. Experiments and computations, in turn, provide a point of confluence and a visual analog for chaotic behavior, multiplicative processes, and scaling behavior. All these concepts have conceptual engineering counterparts: examples arise in the context of flow classification, design of mixing devices, enhancement of transport processes, and controlled structure formation in two-phase systems.

During the past few years there has been considerable interest in dynamical chaos, and examples have been documented among physical, chemical, and biological systems (*1*). Chaos is widespread; in the context of dynamical systems chaos is not the exception but the rule. The technological impact has been less spectacular, however. More often than not, the findings have been a posteriori; that is, explaining ongoing complex behavior and demonstrating that the roots of the complexity can be traced back to a deterministic explanation. There have been recent promising developments in the control of chaos (*2*), and there are instances where keeping a system in a chaotic state might be beneficial. In most practical cases, however, chaos is to be minimized or avoided altogether (*3*). The application of chaos to fluid mixing, however, provides a counterexample to these observations. Fluid mixing is an instance in which chaos is clearly beneficial (*4*). In this article we bring into focus recent theoretical developments and apply them to the interpretation and design of mixing processes in natural sciences and engineering. A few flows, which have become paradigms for mixing studies, are used to exemplify concepts.

Chaos and Symmetry

When stripped of all specific details, mixing can be viewed in purely geometrical terms (*5*). Mixing is intimately bound to the stretching and folding of fluid elements, an idea that can be traced back to a lecture-demonstration by Osborne Reynolds in 1894 (*6*). In turn, stretching and folding constitute the fingerprint of chaos (*5*). Thus, kinematics can serve as template for the evolution of molecular diffusion, chemical reactions, breakup, and aggregation (*7*).

Numerous experimental and computational examples have shown that real fluid flows can produce the type of stretching and folding that leads to chaos (*8–12*). Chaos is impossible in steady, bounded, two-dimensional flows. A steady, two-dimensional flow is completely characterized by time-invariant streamlines that coincide with path lines, and fluid elements lie within the same streamlines for all time. A necessary (but not sufficient) condition for chaos in fluid flows is "streamline crossing" of two streamline portraits taken at arbitrary times. The crossings can create a special type of folding called a horseshoe map, which is one of the signatures of chaos (*5*). Stretching accompanied by this type of folding results in effective mixing within chaotic regions. This is precisely what is accomplished in suitably designed time-periodic flows. Time modulation can be achieved by various means. One possibility, used in flows with low Reynolds numbers (Stokes flows), is to use out-of-phase motion of boundaries; another possibility is to exploit the natural oscillations in flow due to an increase in Rayleigh number as in the case of Rayleigh-Bénard flow (*13*), or the Reynolds number as in the case of Taylor-Couette flow, vortex shedding behind a cylinder (*14*), and other, somewhat more complex, geometries (*15, 16*).

The mixing, however, need not be widespread. In general, poorly mixed regions—islands of regularity, known as Kolmogorov-Arnold-Moser (KAM) tori—coexist with well-mixed chaotic regions. Fluid inside an island can never escape; fluid outside an island can never enter. In spatially periodic systems islands correspond to tubes (Fig. 1).

The mathematical analysis of these concepts is particularly simple in the case of systems represented as maps [time-periodic flows, spatially periodic flows, quasi-periodic systems (*17*), and some classes of three-dimensional flows]. Motion of fluid particles is represented by

$$\mathbf{x}_n = \mathbf{T}^n(\mathbf{x}_0) \tag{1}$$

where n successive applications of the (nonlinear) point transformation $\mathbf{T}$ gives the position of the fluid particle initially located at $\mathbf{x}_0$. A vector $d\mathbf{x}_0$ evolves as

$$d\mathbf{x}_n = D\mathbf{T}^n(d\mathbf{x}_0) \tag{2}$$

where $D\mathbf{T}^n$ represents $\partial T^n_i/\partial x_{0_j}$. The ratio $|d\mathbf{x}_n|/|d\mathbf{x}_0|$ is the length stretch in the interval 0 to n and is denoted $\lambda_{0,n}(\mathbf{x}_0)$. Chaotic flows lead to a distribution of stretchings of the form $\lambda_{0,n}(\mathbf{x}_0) \approx \exp(\sigma n)$, where σ is the short-time Liapunov exponent associated with $\mathbf{x}_0$. Regular, that is, nonchaotic, flows have $\lambda_{0,n}(\mathbf{x}_0) \approx 1 + \kappa n$, where κ is a constant. In time-periodic flows $\lambda_{0,n}$ can be expressed as

$$\lambda_{0,n} = \lambda_{0,1}\lambda_{1,2} \cdots \lambda_{n-1,n} \tag{3}$$

where $\lambda_{i-1,i}$ is the stretching experienced in the interval $i - 1$ to i. Moreover, in chaotic flows, the $\lambda_{i-1,i}$ values quickly become uncorrelated (*18*). These two observations point to a useful connection. Multiplicative processes with weakly correlated steps lead to self-similar distributions; that is, when properly rescaled, the distributions become invariant with respect to time (*19*). Similar behavior is expected of stretching in the chaotic regions of mixing flows.

Chaos is associated with disorder; symmetry with order. However, they can peacefully coexist. Experimental studies have revealed the degree of order and disorder compatible with chaos in fluid flows. Dye structures in time-periodic flows evolve in an iterative fashion; an entire structure is mapped into a new structure with persistent large-scale features, but finer and finer scale features are revealed at each period of the flow (*20*). Thin striations are produced at the expense of thicker ones, and length scales (characterized by a striation thickness, s) decrease exponentially in time. The length stretch and striation thicknesses are inversely related. It is important to stress

J. M. Ottino and S. C. Jana are in the Department of Chemical Engineering, Northwestern University, Evanston, IL 60208. F. J. Muzzio is in the Department of Chemical and Biochemical Engineering, Rutgers University, Piscataway, NJ 08855. M. Tjahjadi is at General Electric Corporate R&D, Post Office Box 8, Schenectady, NY 12301. J. G. Franjione is in the Department of Chemical Engineering, University of Colorado, Boulder, CO 80309. H. A. Kusch is at Chevron Oil Field Research Company, Post Office Box 446, La Habra, CA 90633.

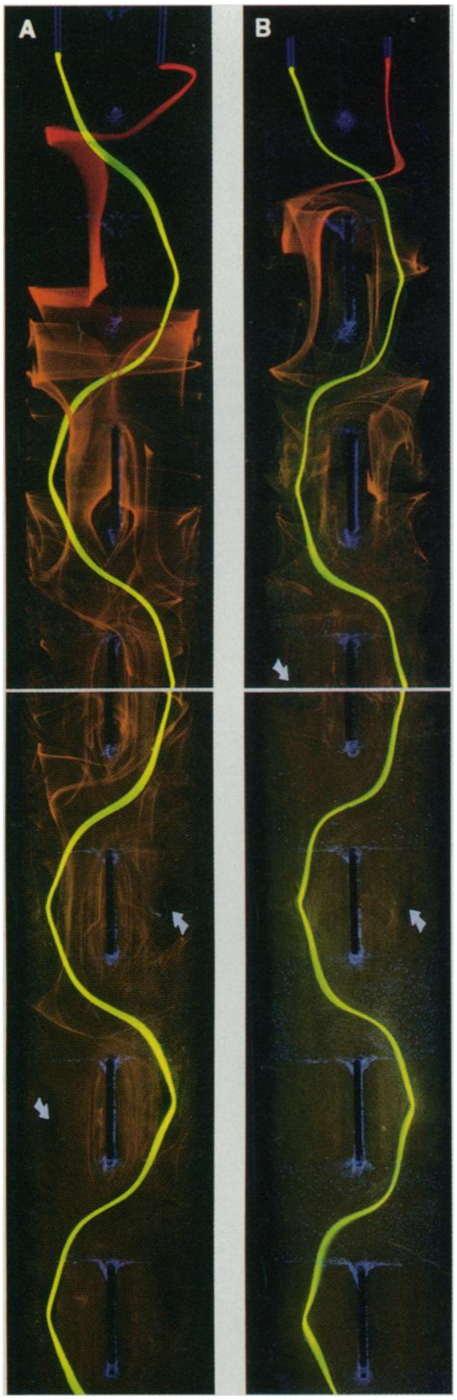

Fig. 1. Coexistence of chaos and regularity in a spatially periodic flow (PPM). The system consists of a pipe partitioned into a sequence of semicircular ducts by means of rectangular plates placed at right angles to each other. The flow is a combination of an axial pressure flow and a cross-sectional drag flow generated by rotation of the pipe relative to the assembly of plates. (**A**) and (**B**) represent two operating conditions. The orange dye is in a chaotic region; the yellow dye is trapped within a KAM tube. Another KAM tube, symmetric to the one shown in the figure, passes through the holes left by the orange dye (marked with white arrows). The orange dye mixes faster in (B) than in (A); however, the shapes of the KAM tubes in both, and (A) and (B), are remarkably similar.

that the length scale reduction for many problems of interest is about 10^4 to 10^5. Thus, in polymer blending the typical reduction is from 10^{-2} to 10^{-6} m, in mixing in the Earth's mantle from 6×10^5 m to about 10^{-1} m, in mixing in the stratosphere from 1×10^6 m to about 10^1 m (*21*), and in the turbulent flow of an agitated chemical reactor from 10^1 m to 3×10^{-5} m (Kolmogorov scales), and from there on to molecular diffusion scales.

Coherent regions of unmixed material (islands) in time-periodic chaotic flows display island symmetry at regular intervals of time (*21, 22*). Island symmetry is caused by symmetric placement of elliptic points (*23*) [a periodic point at **p** means that a particle initially located at **p** returns to **p** after *n* periods, that is, $\mathbf{p} = \mathbf{T}^n(\mathbf{p})$]. Mathematically, two maps **A** and **B** are said to be symmetric to each other if there exists a transformation **S** such that:

$$\mathbf{B} = \mathbf{S}\mathbf{A}\mathbf{S}^{-1} \qquad (4)$$

If $\mathbf{A} = \mathbf{B}$, the symmetry is termed ordinary; if $\mathbf{A}^{-1} = \mathbf{B}$, the symmetry is termed time-reversal. In general, **S** can be rotational symmetry or reflectional symmetry. If a map possesses symmetry, the periodic points are found in symmetric arrangements. As shall be shown later, this knowledge provides a basis for enhancing mixing.

Flows. The most thoroughly studied flows, experimentally and theoretically, are time-periodic closed flows and continuous throughput flows, a special case of which are spatially periodic flows. An example of a closed flow is the time-periodic flow between two eccentric rotating cylinders (*9, 11*); another is a cavity flow with two moving walls (*8, 10*). A computational example is the so-called eggbeater flow (*24*), which can be described as the composition of two shear flows acting on a square (Fig. 2). The first flow acts horizontally for a time T with a velocity field $v(y)$, that is,

$$x_{n+1} = x_n + Tv(y_n),\ y_{n+1} = y_n \qquad (5)$$

and is denoted as $\mathbf{x}_{n+1} = \mathbf{H}\mathbf{x}_n$, where $\mathbf{x} = (x,y)$. The second flow acts in a vertical direction also for time T:

$$x_{n+1} = x_n,\ y_{n+1} = y_n + Tv(x_n) \qquad (6)$$

and is written as $\mathbf{x}_{n+1} = \mathbf{V}\mathbf{x}_n$. In both cases particles leaving through the right side (top) reenter at the left side (bottom). The overall flow is therefore the composition of Eqs. 5 and 6, that is,

$$\mathbf{x}_{n+1} = \mathbf{V}\mathbf{H}\mathbf{x}_n = \mathbf{E}\mathbf{x}_n \qquad (7)$$

Depending on the value of T, the flow can be completely chaotic, completely regular, or anything in between.

Continuous throughput flows are variations on duct flows. Duct flows consist of a two-dimensional cross-sectional flow augmented by a unidirectional axial flow; fluid is mixed in the cross section while it is simultaneously transported down the duct axis. In a duct flow, the cross-sectional and axial flows are independent of both time and distance along the duct axis, and material lines stretch linearly in time (*25*), very much as in two-dimensional steady (or regular) flows. Chaos in duct flows can be achieved by time modulation or by spatial changes along the duct axis (*26*). One example of a spatially periodic duct flow, the partitioned-pipe mixer (PPM), consists of a pipe partitioned with a sequence of orthogonally placed rectangular plates (see Fig. 1). The cross-sectional motion is induced through rotation of the pipe with respect to the assembly of plates, whereas the axial flow is caused by a pressure gradient; the behavior of the system is characterized by the ratio of cross-sectional twist to axial stretching. Other duct flows of technological importance, which possess

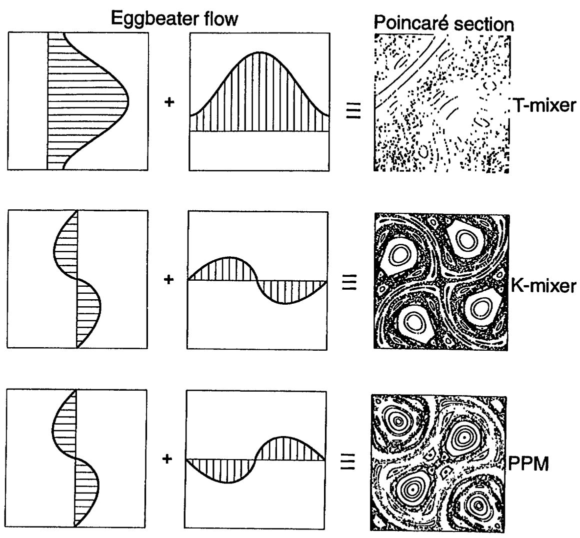

Fig. 2. Eggbeater flows along with representative Poincaré sections and equivalence to spatially periodic flows.

mixing mechanisms similar to the PPM, are the T-mixer [sequences of twisted pipes (27)] and the K-mixer [an idealized version of a static mixer (28)]. Another class of spatially periodic flow is suggested by cavity flows.

Steady cavity flows are poor mixers. The mixing, however, can be significantly improved by means of time-dependent changes in geometry, as shown in Fig. 3 (29). This idea can be readily implemented in the context of duct flows by adding a secondary baffle (see Fig. 3). Such a concept has applications in polymer processing; for example, single screw extruders can be imagined as a channel with a moving lid, very much as in Fig. 3. Similar designs have been arrived at empirically in engineering practice (30).

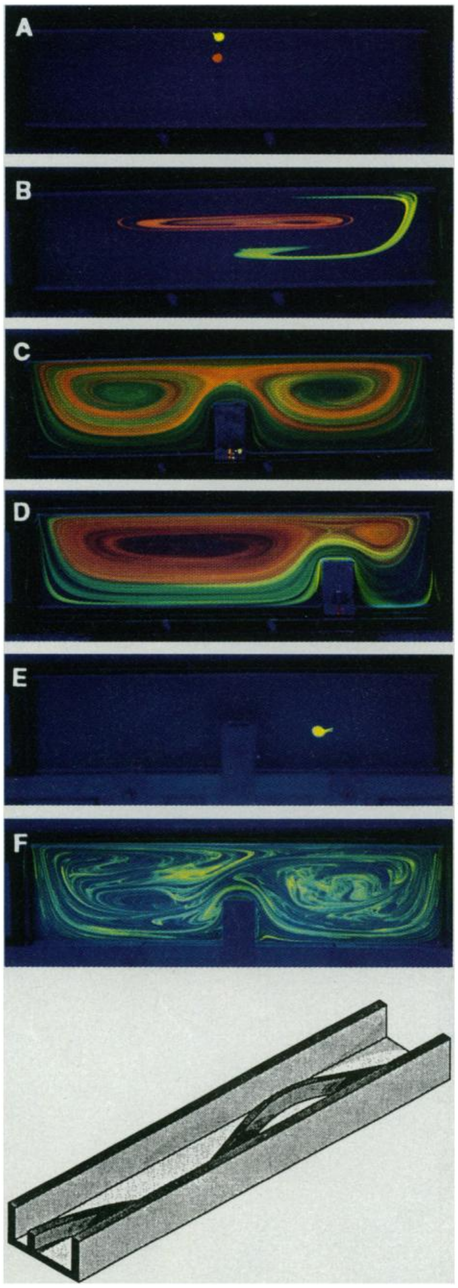

Fig. 3. Mixing improvement by time-periodic changes in geometry. A standard cavity flow, the top boundary moving from left to right, is a poor mixer. The streamlines form closed orbits enclosing a central elliptic point. The initial conditions shown in (**A**) evolve as shown in (**B**) after the top wall has displaced itself 17 times its length. Placement of baffles, as shown in (**C**) and (**D**), changes the streamline portrait radically and a hyperbolic point appears. A periodic change of geometry, (C), (D), (C), mirror image of (D) across the vertical axis, and so on, generates chaotic advection. The initial condition shown in (**E**) evolves into the pattern shown in (**F**) for the same amount of displacement corresponding to case (B). This concept can be readily implemented in continuous throughput flows such as single screw extruder flows. One possibility is to produce a channel with a secondary wavy channel as shown at the bottom of the figure. Cuts at different axial lengths generate streamline portraits such as those of (C) and (D). The mixing shown in (F) can be produced in roughly three periods of the secondary channel.

Stretching and Self-Similarity

Repeated stretching and folding generate self-similarity. There are two types of self-similarity: exact and statistical. Exact self-similarity arises, for example, in the sequences of creases formed by repeated paper folding (31). This type of self-similarity can be condensed in a transformation rule. Statistical self-similarity, on the other hand, is manifested by distributions that exhibit time invariance when plotted in rescaled form (32).

There are two main techniques that can be used to examine statistical self-similarity: single-parameter and multiparameter scaling [also called multifractal scaling (33)]. Single-parameter techniques have been used in the context of mixing, in diffusion and reaction processes, and in breakup in chaotic flows (34), but the bulk of their use so far has been centered in critical phenomena (35) and aggregation processes (36). This technique is well suited for the analysis of the time evolution of probability density functions of λ or $\log\lambda$. Multifractal scaling, on the other hand, has been applied to the fine-scale structure of turbulence (37–39), to model the aggregation probability in clusters generated by diffusion-limited aggregation (40), and to interpret the statistics of scalar fields and the spectrum of finite-time Liapunov exponents in chaotic flows in the limit $t \to \infty$ (18, 41). Multifractals have also been used to describe short-time mixing in a random flow. This technique works well with plots of $\lambda(\mathbf{x},n)$ in flows without islands.

Scaling. Consider a large number of points advected by a flow and let $dN(\lambda)$ be the number of points with stretching between λ and $\lambda + d\lambda$. The probability of a point undergoing a stretch λ after n periods is $F_n(\lambda) = dN(\lambda)/d\lambda$; similarly we can define a probability density function H_n for $\log\lambda$, that is, $H_n(\log\lambda) = dN(\log\lambda)/d(\log\lambda)$. It is apparent that $F_n(\lambda)$ and $H_n(\log\lambda)$ are related by $H_n(\log\lambda) = \lambda F_n(\lambda)$.

A distribution of a variable x at period n, $G_n(x)$, is said to have single-parameter self-similarity (34) if under a transformation of variables

$$x \to y = x/\mathcal{X}(n) \qquad (8)$$

$$G_n(x) \to \mathcal{G}(y) = K(n)G_n(x) \qquad (9)$$

the new function $\mathcal{G}(y)$ becomes (asymptotically) independent of the period n. $\mathcal{X}(n)$ can be obtained as the ratio of two successive convergent moments of $G_n(x)$, $\mathcal{X}(n) = m_i/m_{i-1}$, where the moment m_i is given by

$$m_i(n) = \int_0^\infty x^i G_n(x)dx \qquad (10)$$

$K(n)$ is given by

$$K(n) = C_1\mathcal{X}(n)^2/m_1(n) \qquad (11)$$

where C_1 is a constant. As a result, $\mathcal{G}(y) = \mathcal{X}(n)^2G_n(x)/m_1(n)$

The application of these concepts to $H_n(\log\lambda)$ is straightforward, as shown in Fig. 4. Figure 4B shows that, as n increases, a wider portion of the curves in Fig. 4A

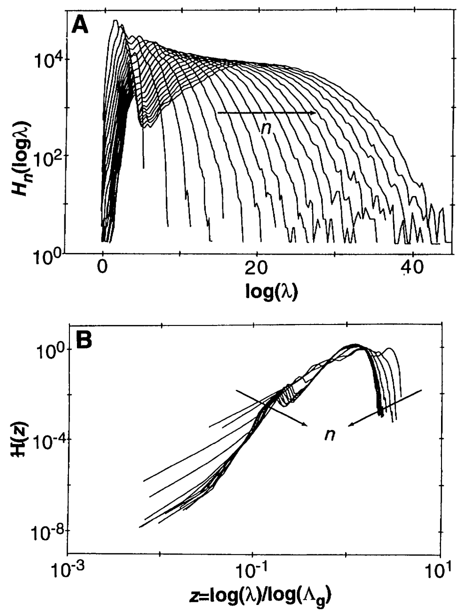

Fig. 4. Single parameter scaling of stretching distributions. (**A**) Typical stretching distribution $H_n(\log\lambda) = dN(\log\lambda)/d(\log\lambda)$ for the flow between eccentric cylinders. (**B**) The curves in (A) nearly overlap when replotted as $\mathcal{H}(z) = (\log\lambda)^2H_n(\log\lambda)/m_{\log\lambda}(n)$, where

$$m_{\log\lambda}(n) = \int \log\lambda H_n(\log\lambda)/d(\log\lambda)$$

is the first moment of $H_n(\log\lambda)$, $z = \log\lambda\log\Lambda_g$, and where Λ_g is the geometric mean stretching, defined as

$\log\Lambda_g =$

$$[\int \log\lambda H_n(\log\lambda)d(\log\lambda)]/[\int H_n(\log\lambda)/d(\log\lambda)]$$

nearly overlap when replotted in scaled form, $\mathcal{H}(z)$. Rigorously speaking, in the limit $n \to \infty$ we have $\lambda_{0,n}(\mathbf{x}_0) \approx \exp(\sigma n)$ for all $\mathbf{x}_0$'s and $\mathcal{H}(z)$ should converge to a delta function, but this does not occur in the short time scales of interest in mixing. In general, we have $m_i \approx m_1(n)^i/m_0(n)^{i-1}$ and, because for the case considered $m_0(n)$ is a constant equal to the number of points considered, N, we have $m_i \approx m_1(n)^i$, which implies that all convergent moments of H_n show an exponential evolution. Thus, uniformity becomes worse before it improves.

Closer examination of the low-z region of $\mathcal{H}(z)$ reveals that there is a set of points that stretch slowly. These points are in the chaotic region, but they remain close to islands for long times (if these points are considered separately from the rest of the population, their λ values exhibit the same type of data collapse when plotted in rescaled form). A general conclusion is that stretching in flows with islands is spatially segregated even in the chaotic regions; one set of points wanders throughout the "bulk of the chaotic region" and undergoes exponential stretching; the other stays close to regular islands for many periods and stretches slowly. These results are important in cases where there are chemical reactions leading to different products according to diffusion-reaction coupling because the overall rate of reaction depends strongly on the spatial distribution of reactants (*42*). The effects of islands (or tubes) extend well into the chaotic regions.

Multifractal scaling yields information regarding the distribution of stretching (*43*). The distribution of finite-time Liapunov exponents, $\sigma(n) = (1/n)\log\lambda_{0,n}$, denoted $P_n(\sigma)$, is expected to scale according to

$$P_n(\sigma) = K_n e^{-ng(\sigma)} \quad (12)$$

where $g(\sigma)$ becomes independent of n for $n \to \infty$ (*33*). Because $\sigma(n) = (1/n)\log\lambda_{0,n}$, $dN(\sigma) = dN(\log\lambda)$, and $d\sigma = (1/n)d\log\lambda$, after normalization and application of the "method of steepest descent" we obtain (*43*)

$$P_n(\sigma) = ndN(\log\lambda)/d\log\lambda \sim nH_n(\log\lambda)/N \sim n^{1/2}e^{-n[g(\sigma)-g(\sigma_m)]} \quad (13)$$

Therefore, a plot of $(1/n)\log[n^{1/2}H_n(\log\lambda)]$ versus $(1/n)\log(\lambda)$ should produce a time-independent function $h(\sigma) = -[g(\sigma) - g(\sigma_m)]$, where σ_m corresponds to the maximum of $h(\sigma)$. As shown in Fig. 5, curves for different times indeed collapse onto a single curve when this scaling is applied. This behavior verifies that Eq. 13 produces an almost invariant $h(\sigma)$ for flows without islands. Furthermore, the parabolic shape of the curves in Fig. 5 indicate that the stretching is log-normally distributed, that is,

$$H_n(\log\lambda) \sim n^{-1/2}e^{-[(\log\lambda - n\sigma_m)^2/n]} \quad (14)$$

Mixing Enhancement by Symmetry Control

Symmetries provide means of classifying and manipulating complex flows. Symmetries exist whenever there are constraints on the velocity field: in Stokes flows these can be the result of geometrical constraints; in other cases they might be dictated by the evenness or oddness of the velocity field. Symmetries in simple analyzable flows can act as a template for the classification of more complex flows. Consider, for example, the application of these ideas to the eggbeater flow with even velocity field in both $\mathbf{H}$ and $\mathbf{V}$ (see Fig. 2). In this case we have

$$\mathbf{V} = \mathbf{RHR}^{-1} \quad (15)$$

where $\mathbf{R}$ represents a 90° rotation; that is, $(x,y) \to (-y,x)$. Moreover, because $\mathbf{R}$ itself is symmetric to its inverse with respect to reflections across the x axis, $\mathbf{R} = \mathbf{S}_x\mathbf{R}^{-1}\mathbf{S}_x$ and $\mathbf{H}$ is symmetric about the x axis; $\mathbf{H} = \mathbf{S}_x\mathbf{H}\mathbf{S}_x$, then

$$\mathbf{VH} = \mathbf{RS}_x\mathbf{HS}_x\mathbf{R}^{-1}\mathbf{H} = \mathbf{S}_1\mathbf{HS}_1\mathbf{H} = (\mathbf{S}_1\mathbf{H})^2 \quad (16)$$

where $\mathbf{S}_1 = \mathbf{RS}_x$, $\mathbf{S}_1$: $(x,y) \to (y,x)$, that is, a reflection about the 45° line. Extension of this line of analysis suggests the introduction of a family of generalized eggbeater flows, in which the directions, forward (+1) or inverse (−1) of $\mathbf{R}$ and $\mathbf{H}$, and the evenness (e) or oddness (o) of the velocity field v are unspecified. This pattern/symmetry leads to maps of the form $\mathbf{R}^{\pm1}\mathbf{H}_{e/o}{}^{\pm1}\mathbf{R}^{\pm1}\mathbf{H}_{e/o}{}^{\pm1}$, which translates into 32 different flows. However, only four of these are independent and each is associated with different symmetries; each acts as a template for the classification of more realistic flows. For example, there is a one-to-one correspondence between these flows and several spatially periodic flows (*25*), such as the PPM, the K-mixer, and the T-mixer (see Table 1 and Fig. 2).

Probably the most general question that can be asked regarding mixing is: What flow is capable of generating the most effective mixing while consuming the minimum amount of energy? In engineering terms, this question might be posed as: How should impeller size and geometry be chosen? What is the optimum sequence of elements for a static mixer? or What is the optimum placement of pins in an extruder channel? The answers to these questions are quite specific and require considerable investment in experiments or computer calculations while yielding no real conceptual insight. Consideration of symmetry of flows allows a reduction of the problem to a more tractable, albeit less rigorous, one but also allows a theoretical basis for geometrical intuition regarding mixing. Symmetry in chaotic flows stems from underlying geometric constraints on fluid motion. Roughly, if there is a line of symmetry in a flow, then it is also known that poorly mixed regions will be located in symmetric arrangements with respect to the line (see Fig. 2). Any periodic sequence of flows will possess symmetry. Thus, it is possible to alter the location of the symmetry lines by changing the flow; and this in turn changes the location of poorly mixed regions resulting in an overall effective flow. These concepts have

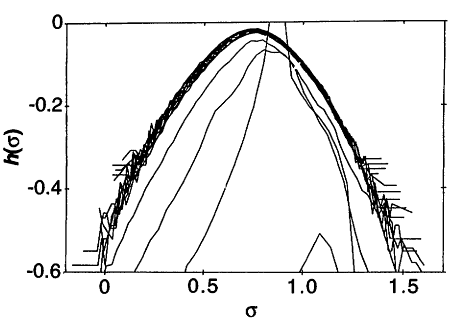

Fig. 5. Scaling of finite-time Liapunov exponents in the eggbeater flow with $T = 3$ corresponding to $n = 1, 2, 4, 8, 16$ to 30 periods.

Table 1. Symmetries provide means of classifying and manipulating complex flows represented as maps. The eggbeater flow can be expressed as a composition of two 90° rotations; $\mathbf{R}$: $(x, y) \to (-y, x)$, and maps representing simple shear, $\mathbf{H}_e$, $\mathbf{H}_o$, according to whether the velocity profile is either even (e) or odd (o). Equivalently, as the second iterate of a reflection about the 45° line; $\mathbf{S}_1$: $(x, y) \to (y, x)$, and either $\mathbf{H}_e$ or $\mathbf{H}_o$. Similarly, several kinds of constant throughput flows can be represented by compositions of rotations, $\mathbf{R}$, and a transformation representing the effect of Poiseuille flow, $\mathbf{F}_o$. Three of the four fundamental eggbeater flows correspond to common, continuous, throughput flows.

Fundamental eggbeater flow	t-reversal	Ordinary	Continuous throughput flows	Equivalent maps
$\mathbf{RH_eR^{-1}H_e = (S_1H_e)^2}$	−45°	None	T-mixer	$\mathbf{R^{-1}F_0{}^{-1}RF_0}$
$\mathbf{RH_eRH_e = (RH_e)^2}$	−45°	None		
$\mathbf{RH_o{}^{-1}R^{-1}H_0 = (S_1H_0)^2}$	±90°	180°	K-mixer	$\mathbf{R^{-1}F_0{}^{-1}RF_0}$
$\mathbf{RH_0RH_0 = (RH_0)^2}$	±45°	180°	PPM	$\mathbf{R^{-1}F_0RF_0}$

been incorporated in both experimental and numerical analysis of mixing in two- and three-dimensional viscous flows (24, 25). Results indicate that, although time-periodic or spatially periodic flows can yield effective mixing, poorly mixed regions exist, and the prediction of the exact locations and the sizes of these regions is a daunting task. Consideration of symmetry indicates that aperiodic sequences, although not necessarily optimal, generate more effective mixing compared with the corresponding periodic sequence.

Consider briefly the application of these ideas to the eggbeater flow with 45° and −45° symmetry lines (see Table 1 and Fig. 2). In order to improve mixing, we "rotate the flow" by 90°; that is, we follow the flow **VH** with $\mathbf{R}[\mathbf{VH}]\mathbf{R}^{-1} = \mathbf{HV}$. In the **HV** flow, then, the two symmetry lines will switch places relative to their positions in the **VH** flow, that is, structures that were located on the 45° line in the **VH** flow will now be found on the −45° line in the **HV** flow. The sequences of actions can be written as:

$$\mathbf{P}_{n+1} = \mathbf{R}\mathbf{Q}_n\mathbf{R}^{-1} \text{ with } \mathbf{Q}_n = \mathbf{P}_n\mathbf{P}_{n-1} \ldots \mathbf{P}_0 \text{ and } \mathbf{P}_0 = \mathbf{VH} \quad (17)$$

This generates the sequence **VH** ($n = 0$), **HVVH** ($n = 1$), **VHHVHVVH** ($n = 2$), and **HVVHVHHVVHHVHVVH** ($n = 3$) [note that the **H**'s and **V**'s follow the transformation **V** → **VH**; **H** → **HV**; this sequence is called the Morse-Thue sequence; it is aperiodic but it is clearly not random (31)]. This concept can be readily implemented in duct flows (24). In its most developed state, symmetry can be used to develop rules of thumb regarding the most effective sequences of flows (for example, geometrical arrangements of elements in a static mixer, or placement of baffles in channel or tank mixing).

Transport Enhancement

Chaos is an effective transport aid. At small scales, stretching and folding smooth out concentration fluctuations; at global scales, chaos shuffles large portions of fluid (44) and thereby produces global uniformity and increased transport between walls and bulk fluid (45).

Molecular interdiffusion is controlled by stretching. Stretching increases the area available for interdiffusion and reduces diffusional length scales, s. Because both are related ($s \sim 1/\lambda$), the effect of stretching on molecular diffusion goes as λ^2 (46). Moreover, stretching provides a glimpse into the character of striation thickness distributions. Because the length achieved by a material element is proportional to its stretch, the number of striations with thickness s, $dN(s)$, is proportional to the total stretch, that is, $dN(s) \sim \lambda dN(\lambda)$. Equivalently, because $s \sim 1/\lambda$, $s dN(s) \sim dN(\lambda)$, and

$$F_n(\lambda) \sim s^3 dN(s)/ds \quad (18)$$

$$H_n(\log\lambda) \sim s^2 dN(s)/ds \quad (19)$$

This result can also be justified as follows: If we divide the flow into small boxes, the total intermaterial area in a box is proportional to λ. The average thickness in the box is $\langle s \rangle \sim 1/\lambda$, and each box contains a number of striations proportional to λ. Therefore, the number of striations with thickness $\langle s \rangle$, $dN(s)$, is equal to $dN(\lambda)$, times the number of striations per box. This again leads to $dN(s) = \lambda dN(\lambda)$ and $dN(s)/ds = \lambda^3 dN(\lambda)/d\lambda$.

For flows without islands, a log-normal $H_n(\log\lambda)$ (Eq. 19) leads immediately to an s distribution of the form

$$f(s,t) \sim \lambda^2 \exp[-(\log s - \log\langle s \rangle)^2/Kt] \quad (20)$$

where $\langle s \rangle$ is the mean striation thickness (47). The standard deviation of the distribution, Kt, increases linearly in time; this relation suggests that unmixed regions persist for long times.

The order of contact of the striations matters as well; one such case is when there are diffusion and diffusion-controlled chemical reactions of the form A + B → P. Reaction occurs at planes between striations and thin lamellae are consumed by thicker neighbors, which merge themselves into thicker domains. This process results in a time-evolving distribution of striation thicknesses. It has been shown, however, that different initial striation thickness distributions (for example, random, normal, or other) evolve asymptotically into the same limiting distribution (48, 49). Other cases might be less forgiving. For example, in moderately fast reactions of the form A + B → P, P + B → R, the time evolution and the final ratio of the amounts of the two products, P/R, depend on the precise way in which the fluids are mixed (45).

More generally, the extent to which the transport is affected by stretching depends on the ratio between the rate of mixing and the speed of molecular diffusion. Diffusion and convection occur in parallel, and, depending on the conditions, one might dominate over the other. Idealized stretching and shuffling mechanisms highlight these competing effects. Consider the case of one-dimensional heat diffusion into a fluid thread whose boundaries are maintained at constant temperature and two shuffling mechanisms. In mechanism I, which mimics the stretching and folding present in chaotic flows, a thread of thickness 1 is stretched by a factor of 2, cut into two, and the pieces are glued together to restore the original thickness; in mechanism II, the thread is cut into halves, flipped, and glued together (Fig. 6A). Diffusion occurs after each shuffling step. Because the stretching and cutting are instantaneous, the processes are described by

$$\partial\theta/\partial t = \partial^2\theta/\partial x^2 \quad (21)$$

$$\theta(x,0) = 0,\ \theta(-1,t) = \theta(1,t) = 1 \quad (22)$$

where θ is dimensionless temperature, t is dimensionless time, and x is dimensionless distance. With diffusion alone, the fluid reaches an average temperature of 1/2 at $t = 0.0485$; we take this value of t as the upper limit of heating time, t_{max}.

Which shuffling mechanism is more efficient, I or II? What is the best cutting policy? That is, if only N cuts are allowed in time t_{max}, how should the cuttings be distributed? To simplify matters, consider the following time cutting rules:

$$t(i) = t_{max}(i/N)^a \quad (23a)$$

$$t(i) = t_{max}(1 - i/N)^a \quad (23b)$$

where $t(i)$ is the time for the ith cut and a determines the density of cuts ($a = 1$ corresponds to uniform cut times). Equation 23a represents type A cuts (dense at the beginning) whereas Eq. 23b represents type B cuts (dense towards the end). The time between two consecutive, t_c, cuts is $t(i) - t(i-1)$, with $t(0) = 0$. Even in this simple framework, several cutting policies come to mind: AB (first $N/2$ cuts are of type A up to a time $t_{max}/2$, type B for the rest of the time); AA (first $N/2$ cuts of type

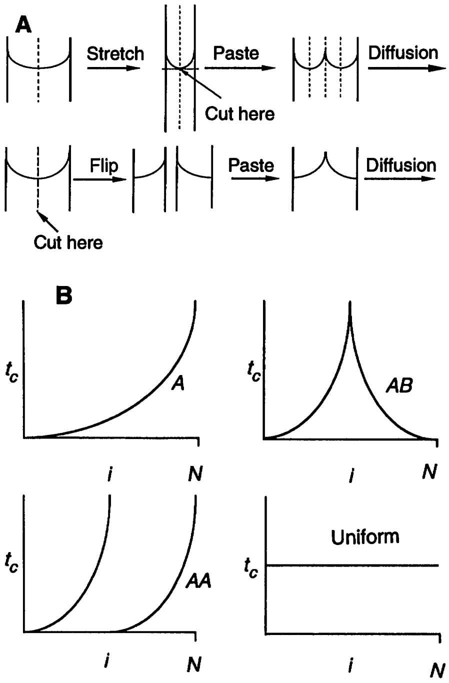

Fig. 6. (**A**) Effect of stretching-and-cutting and cutting-and-flipping mechanisms on one-dimensional heat diffusion. (**B**) Cutting time policies: type A, AB, AA, and uniform.

A up to a time $t_{max}/2$, followed by type A cuts started again for the rest of the time), and so on (Fig. 6B).

Simulations reveal that the stretching-and-cutting mechanism is more efficient than the cutting-and-flipping mechanism. Between two consecutive cuts, heat diffuses into the material, reducing the temperature gradient at the wall. With stretching, this slowing down is more than compensated for by the increase in the gradient due to stretching. In the flipping mechanism, on the other hand, the wall temperature gradient is determined by the temperature at the center of the fluid, which increases gradually, leading to the decrease of the flux at the wall. This supports the notion that chaos—stretching and folding—is an efficient transport enhancement mechanism.

Numerical examination of the various cutting policies shown in Fig. 6 shows that distributions with fast initial cuttings are better; distribution A is the best, AA and AB are the second best, uniform cutting times are third, BA and BB are fourth, and B is the least efficient. Equally spaced cutting times are bad because most of the heating occurs at the beginning and only a few cuttings are made during that time. On the other hand, initial cuttings that are too fast are not good because only a thin layer of fluid is heated in such a short time, and cuttings are wasted in shuffling much of the cold fluid within themselves. The best result with policy A corresponds to $a \approx 4$.

More elaborate examples show similar behavior but also new physics. For example, the heating of a Newtonian fluid in a rectangular cavity using time-periodic flows reveals similar trends (50). Péclet numbers play the role of cutting times (the Péclet number measures the rate of transport of heat by advection to the rate of transfer by conduction, and is defined as $Pe = VL/\alpha$, where V and L are characteristic velocity and time scales, respectively, and α is the thermal diffusivity of the fluid). At low Péclet numbers the thermal diffusion dominates and chaos plays almost no role. At large Péclet numbers a thin thermal boundary layer is formed at the walls; however, this is precisely the region where the flow is typically less chaotic, and thus the effect of chaotic advection is reduced to shuffle portions of materials in a center region where the temperature is already uniform. The best results are obtained at intermediate Péclet numbers; the temperature gradient is spread over a wider chaotic region and the shuffling action of the chaotic advection, taking parcels of hot fluid from the wall region and replacing it by cold center-region fluid, enhances the rate of heating considerably (Fig. 7).

More practical application of these concepts is also possible. A possible example is the enhancement of transport away from surfaces containing small cavities, wedges, and indentations, as in the cleaning of surfaces in microelectronic applications, or from pores connecting two fluids, such as in membranes subject to flow. Such flows, for low Reynolds numbers, lead to cells or a succession of cells of diminishing strength (51). The transport can be substantially increased if the flow is made chaotic. One such illustration is the removal of an impurity initially trapped in a deep open cavity by a jet whose angle is changed in a time-periodic manner. The process occurs in two stages. Most of the particles above a dividing KAM surface are removed within a few periods; the rest are removed by molecular diffusion and leakage through the KAM surface on a longer time scale.

Flow Structuring

Chaotic flows can be used to aggregate or to break and disperse. Experiments are available in the case of fragmentation and dispersion of viscous drops (52); studies of aggregation are at a computational level (53, 54).

Aggregation in chaotic flows is faster and goes further than in regular flows. In the simplest scenario, particles are initially placed randomly throughout the flow and coagulate, preserving their size. When two clusters get closer than a capture diameter d, they coagulate into a cluster whose mass is the sum of the two; this process results in a distribution of cluster masses. In regular flows coagulation stops because particles become segregated (55); however, no such limitation exists in the case of chaotic flows with disconnected islands. Clusters are kept well mixed by the chaotic flow (56), and the final result is a single cluster encompassing all particles. The cluster mass distribution is self-similar with respect to time (57).

Somewhat more complex is the case where particles bond rigidly to form growing clusters that move as units. Chaotic flow, in this case, creates fractal aggregates reminiscent of those formed by diffusion-limited aggregation (58) and suggests possibilities for tailoring of fractal structures by fluid flow.

The case of drop elongation and breakup is a bit more complex. The simplest case corresponds to drops that do not interact with each other (Fig. 8). Under supercritical conditions—capillary numbers above their critical value—droplets elongate into long filaments that break by flows driven by surface tension. This process results in a wide distribution of drop sizes (34). When properly scaled, drop size

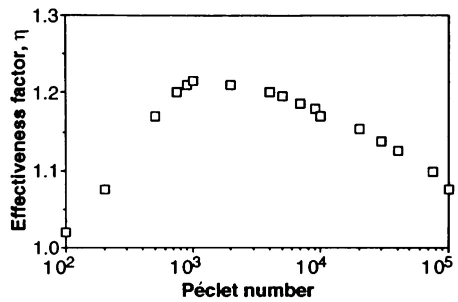

Fig. 7. Enhancement factor (η) as a function of Péclet number for N_d = 16 with D = 0.1 for heating of a fluid in a closed square cavity using square wave-form wall motions. The total wall displacement, N_d, is defined as the product of the wall displacement per period, D, and the total number of periods, P; $N_d = DP$. The enhancement factor is defined as the ratio of the average temperature of the fluid using the chaotic flow to that produced by the application of the regular flow for the same value of N_d (N_d is a measure of the cost incurred in moving the walls). The best results are obtained at intermediate Péclet numbers.

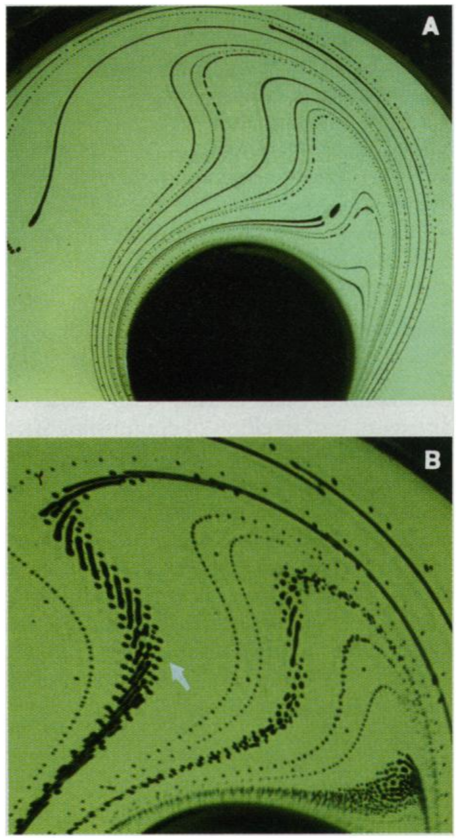

Fig. 8. Stretching, folding, and breakup of a fluid filament advected by a chaotic flow. In (**A**) the drops break by capillary wave instabilities; further stretching separates the droplets, which essentially behave independently of each other. In (**B**) breakup occurs as the filament is being contracted; droplets in the process of being broken become stacked up as in the region marked with the white arrow.

distributions corresponding to different operating conditions and different viscosity ratios collapse into a single scaling curve.

An understanding of these results relies on stretching and folding at large scales, on one hand, and on the details of fragmentation processes driven by surface tension of small scales, on the other. Experimental and computational investigations of the details of the breakup of a fluid filament reveal that drops are generated because of multiple breakup sequences around the neck region of a highly deformed filament (59). The largest drops are called mother drops; the other drops are referred to as satellites. Each pinch-off is associated with the formation of a neck, and the neck undergoes pinch-off; the mechanism is self-repeating.

These ideas can be used to predict the drop size distribution observed in experiments (52). Under appropriate conditions, drop stretching is passive: the increase in length of the fluid filament is identical to the stretch of a material element located at the center of the drop. Spherical drops of volume $(4/3)\pi r_0^3$ stretch into a filament of length λ and cross-sectional radius $r_0/\lambda^{1/2}$. Assume that such filaments break into N mother drops of radius $r = c_0/\lambda^{1/2}$, where c_0 is nearly constant and proportional to r_0. Mass conservation requires $N = (r_0/r)^3 \approx \lambda^{3/2}$. As a result, the total number of drops of radius r is given by $dN(r) \approx \lambda^{3/2}dN(\lambda)$. If we assume again that the distribution of stretching values is log-normal, the mother drop radii follows

$$dN(r)/dr \approx r^{-3}(K\pi n)^{-1/2} \exp\{-(n/K)[(\log c_0 - 2 \log r)/\sigma_m^2]\} \quad (24)$$

In addition, each mother drop carries a distribution of satellites of diminishing size. Each mother drop of radius r has associated one large satellite of radius $r^{(1)}$, two smaller satellites of radius $r^{(2)}$, four satellites of radius $r^{(3)}$, and so on. Equation 24 can be used to predict the drop size distribution of all satellites, and the different predictions can be used to predict the overall drop size distribution (mother drops and satellites). Calculations show good qualitative agreement with experiments.

Conclusions

There is little doubt that chaos-based concepts can be used in the context of engineering applications (60). This article has focused on examples involving mixing and transport in viscous fluids. Many other possibilities are open, and further exploration is warranted. It is also apparent, however, that clear-cut engineering applications are unlikely to emerge in ready-made form. The burden is now on engineers to adapt and modify what is already available or to develop new concepts and ideas. It should be also clear that the uses of chaos concepts should not be confined to the invention of new processes. The knowledge that chaos exists should provide a new way of examining existing processes and a foundation for empirical designs and rules of thumb.

REFERENCES AND NOTES

1. C. Grebogi, E. Ott, J. A. Yorke, *Science* **238**, 632 (1987); M. V. Berry, I. C. Percival, N. O. Weiss, *Dynamical Chaos* (Royal Society, London, 1987); also published in *Proc. R. Soc. London Ser. A* **413** (no. 1844), 1–199 (1987); J. M. T. Thompson, *Appl. Mech. Rev.* **42**, 15 (1989).
2. T. Shinbrot *et al.*, *Phys. Rev. Lett.* **68**, 2863 (1992); T. Shinbrot, E. Ott, C. Grebogi, J. A. Yorke, *ibid.* **65**, 3215 (1990); *Phys. Rev. A.* **45**, 4165 (1992); W. L. Ditto, S. N. Russo, M. L. Spano, *Phys. Rev. Lett.* **65**, 3211 (1990); R. Lima and M. Pettini, *Phys. Rev. A* **41**, 726 (1990).
3. M. P. Golden and B. E. Ysdtie, *Automatica* **28**, 11 (1992).
4. R. Pool, *Science* **250**, 626 (1990).
5. J. M. Ottino, *The Kinematics of Mixing: Stretching, Chaos, and Transport* (Cambridge Univ. Press, Cambridge, 1990).
6. O. Reynolds, *Nature* **50**, 161 (1894).
7. J. M. Ottino, *Phys. Fluids A* **5**, 1417 (1991).
8. W. L. Chien and J. M. Ottino, *J. Fluid Mech.* **170**, 355 (1986).
9. J. Chaiken, R. Chevray, M. Tabor, Q. M. Tan, *Proc. R. Soc. London Ser. A* **408**, 165 (1986).
10. C. W. Leong and J. M. Ottino, *J. Fluid Mech.* **209**, 463 (1989).
11. A combined experimental and computational study appears in P. D. Swanson and J. M. Ottino, *ibid.* **213**, 227 (1990).
12. Computational work appears in H. Aref, *ibid.* **143**, 165 (1986); D. V. Khakhar, H. Rising, J. M. Ottino, *ibid.* **172**, 419 (1986); A. Crisanti, M. Falcione, A. Vulpiani, *Nuovo Cimento* **14**, 1 (1991).
13. T. H. Solomon and J. P. Gollub, *Phys. Rev. A* **38**, 6280 (1988).
14. K. Shariff, T. H. Pulliam, J. M. Ottino, *Lect. Appl. Math.* **28**, 613 (1991).
15. G. E. Karniadakis, I. G. Kevrekidis, Z.-H. Shen, A. J. Smits, *Phys. Fluids A* **3**, 1063 (1991).
16. The Reynolds number is defined as VL/v; the Rayleigh number is defined as $\gamma g L^3 \Delta T/(\alpha v)$ (V, L, and ΔT are characteristic velocity, length, and temperature difference, respectively; g is the acceleration of gravity; v is the kinematical viscosity; γ is the coefficient of thermal expansion; and α is the thermal diffusivity).
17. D. Beige, A. Leonard, S. Wiggins, *Nonlinearity* **4**, 775 (1991).
18. F. J. Muzzio, P. D. Swanson, J. M. Ottino, *Phys. Fluids A* **5**, 822 (1991).
19. S. Redner, *Am. J. Phys.* **58**, 267 (1990).
20. J. M. Ottino, *Sci. Am.* **260**, 56 (January, 1989).
21. M. N. Juckes and M. E. McIntyre, *Nature* **328**, 590 (1987).
22. J. M. Ottino, C. W. Leong, H. Rising, P. D. Swanson, *ibid.* **333**, 419 (1988).
23. J. G. Franjione, C. W. Leong, J. M. Ottino, *Phys. Fluids A* **1**, 1772 (1989).
24. J. G. Franjione and J. M. Ottino, *Philos. Trans. R. Soc. London* **338**, 301 (1992).
25. ______, *Phys. Fluids A* **3**, 2819 (1991).
26. H. A. Kusch and J. M. Ottino, *J. Fluid Mech.* **236**, 319 (1992).
27. S. W. Jones, O. M. Thomas, H. Aref, *ibid.* **208**, 335 (1990).
28. S. Middleman, *Fundamentals of Polymer Processing* (McGraw-Hill, New York, 1977).
29. The first experiments of this kind are due to C. W. Leong, University of Massachusetts (1988).
30. C. Rauwendaal, *Mixing in Polymer Processing* (Dekker, New York, 1991).
31. M. Schroeder, *Chaos, Fractals, Power Laws* (Freeman, New York, 1991).
32. F. J. Muzzio, P. D. Swanson, J. M. Ottino, *Int. J. Bifurcations Chaos Appl. Sci. Eng.* **2**, 37 (1992).
33. M. A. Sepúlveda, R. Badii, E. Pollak, *Phys. Rev. Lett.* **63**, 1226 (1989).
34. F. J. Muzzio, M. Tjahjadi, J. M. Ottino, *ibid.* **67**, 54 (1991).
35. P. C. Hohenberg and B. I. Halperin, *Rev. Mod. Phys.* **49**, 435 (1977).
36. P. Meakin, in *Phase Transitions and Critical Phenomena*, C. Domb and J. L. Lebowitz, Eds. (Academic Press, New York, 1988), vol. 12, pp. 335–488, and references therein.
37. U. Frisch and G. Parisi, in *Turbulence and Predictability in Geophysical Fluid Dynamics*, N. Ghil, R. Benzi, G. Parisi, Eds. (North-Holland, Amsterdam, 1985), pp. 84–88.
38. C. Meneveau and K. R. Sreenivasan, *J. Fluid Mech.* **224**, 429 (1991); K. R. Sreenivasan and C. Meneveau, *Phys. Rev. A* **38**, 6287 (1988).
39. T. C. Halsey, M. H. Jensen, L. P. Kadanoff, I. Procaccia, B. Shraiman, *Phys. Rev. A* **33**, 1141 (1986).
40. A. Coniglio, *Physica A* **140**, 51 (1986).
41. E. Ott and T. M. Antonsen, *Phys. Rev. Lett.* **61**, 2839 (1988); F. Városi, T. M. Antonsen, E. Ott, *Phys. Fluids A* **3**, 1017 (1991).
42. F. J. Muzzio and J. M. Ottino, *Phys. Rev. Lett.* **63**, 47 (1989).
43. F. J. Muzzio, C. Meneveau, P. D. Swanson, J. M. Ottino, *Phys. Fluids A* **4**, 1439 (1992).
44. V. Rom-Kedar, S. Wiggins, A. Leonard, *J. Fluid Mech.* **214**, 347 (1990).
45. An analytical study in the context of the flow between two eccentric cylinders appears in S. Gosh, H. C. Chang, M. Sen, *J. Fluid Mech.* **238**, 119 (1992); an experimental study in the context of the T-mixer appears in N. Acharya, M. Sen, H. C. Chang, *Int. J. Heat Mass Transfer*, in press.
46. R. Chella and J. M. Ottino, *Chem. Eng. Sci.* **38**, 551 (1984).
47. The distribution of striation thicknesses has been measured for the flow between cylinders (W. J. A. Dahm, University of Michigan, personal communication). A fitting of the data shows good qualitative agreement with a log-normal distribution.
48. F. J. Muzzio and J. M. Ottino, *Phys. Rev. A* **40**, 7182 (1989); *ibid.* **42**, 5873 (1990).
49. I. M. Sokolov and A. Blumen, *ibid.* **43**, 2714 (1991); *ibid.*, p. 6345.
50. S. C. Jana and J. M. Ottino, *Philos. Trans. R. Soc. London* **338**, 519 (1992).
51. H. K. Moffatt, *J. Fluid Mech.* **18**, 1 (1964).
52. M. Tjahjadi and J. M. Ottino, *ibid.* **232**, 191 (1992).
53. F. J. Muzzio and J. M. Ottino, *Phys. Rev. A* **38**, 2516 (1988).
54. T. J. Danielson, F. J. Muzzio, J. M. Ottino, *Phys. Rev. Lett.* **66**, 3128 (1991).
55. F. J. Muzzio, thesis, University of Massachusetts, Amherst (1991).
56. U. R. Bidkar and D. V. Khakhar, *Phys. Rev. A* **42**, 5964 (1990).
57. P. G. J. van Dongen and M. H. Ernst, *J. Stat. Phys.* **50**, 295 (1988).
58. P. Meakin, in *On Growth and Form: Fractal and Non-Fractal Patterns in Physics*, H. E. Stanley and N. Ostrowsky, Eds. (Nijhoff, Dordrecht, 1985), pp. 111–135.
59. M. Tjahjadi, H. A. Stone, J. M. Ottino, *J. Fluid Mech.*, in press.
60. Recent examples include P. H. M. Elemans, thesis, Technical University Eindhoven, Netherlands (1989); H. E. H. Meijer and J. M. H. Janssen, in *Mixing and Compounding—Theory and Practice*, I. Manas-Zlocower and Z. Tadmor, Eds., G. Fritz, series editor (Hanser, Munich, in press), chap. I, sect. I.4.

61. This research was supported by the Department of Energy (Office of Basic Energy Sciences), the Air Force Office of Scientific Research, and the National Science Foundation, Division of Fluid Mechanics.